The pressure and velocity dependence of flow-type cavitation erosion

J.G. Auret[a], O.F.R.A. Damm[b], G.J. Wright[a] and F.P.A. Robinson[b],*

[a]*Division of Materials Science and Technology, CSIR, P.O. Box 395, Pretoria 0001 (South Africa)*
[b]*University of the Witwatersrand, P.O. WITS 2050 (South Africa)*

Abstract

Previous results on the influence of water pressure and velocity on flow-type cavitation erosion, *i.e.* an increase in erosion rate with increasing velocity and peaking of erosion rate as a function of pressure, were confirmed by measurements with a rotating-disc test rig.

Owing to the importance of exercising control over the cavitation geometry in hydraulic equipment, the effect of pressure and velocity on the position and shape of the cavitation erosion zone was systematically studied. The observed geometry of the erosion zone, as well as the wear rate behaviour, was explained in terms of the change in the cavitation-inducing pressure gradient with pressure and velocity.

1. Introduction

Cavitation occurs when relative movement between a solid object immersed in a liquid and the liquid creates low pressure regions in the liquid, leading to localized rapid vaporization. The collapse of these vapour pockets or bubbles happens extremely quickly and may lead to damage to nearby solid objects. This form of damage is known as cavitation erosion. Flow-type cavitation erosion is caused by unidirectional relative movement between the liquid and the solid object (*e.g.* a ship's screw), as opposed to vibratory cavitation erosion.

For flow-type cavitation erosion, well-defined relations exist between the flow velocity and liquid pressure, and the amount of cavitation and erosion damage. Experimental work using a variety of cavitation test rigs has been reported. The influence of pressure was investigated both in venturi-type [1–6] and vibratory [7–11] test rigs. Erosion rate as a function of pressure shows a maximum as illustrated in Fig. 1. The drop-off at the low pressure side is ascribed to a decrease in bubble collapse violence as a result of the smaller pressure differential. At pressures above the maximum damage rate, the minimum pressure rises and therefore fewer bubbles can nucleate.

Water tunnels [12–13], venturi-type [1–2,14] and rotating disc-type [15–17] test devices were used to evaluate the effect of velocity. Damage usually increases
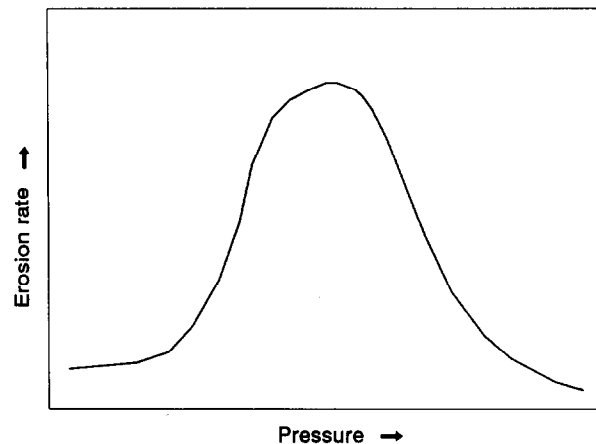

Fig. 1. Profile of cavitation erosion rate as a function of pressure.

with a power of the velocity ranging between five and ten, although negative powers have been observed under well-developed cavitation conditions where the pressure becomes insensitive to velocity changes.

Although numerous investigators studied the nature of the cavitation field by *in situ* observation [18–19] and the damage mechanisms operating on eroding surfaces [20–21], little information has been published on the relation between cavitation and erosion geometries, and especially the influence of fluid and flow parameters on these. However, an understanding of this relationship is critical in hydraulic devices operating under cavitation-inducing conditions, as the design and

---

*Professor of Corrosion Science and Engineering

operating conditions of such devices can be tailored to minimize damage by displacing the cavitation zone to less critical areas [22].

The relation between velocity and pressure, and cavitation and damage characteristics has been the subject of the present study. It is shown that both the amount and location of the damage can be understood in terms of the pressure profile behaviour.

2. Experimental procedure

2.1. Cavitation erosion test rig

A rotating-disc test rig [15–16,23–25] was designed and built for the experimental work (Fig. 2). The rig facilitated the investigation of cavitation dynamics as well as erosion resistance under the conditions showed in Table 1.

The disc could contain three rectangular or three round samples on either side, as shown in Fig. 3. A maximum of three inducer holes were exposed at any
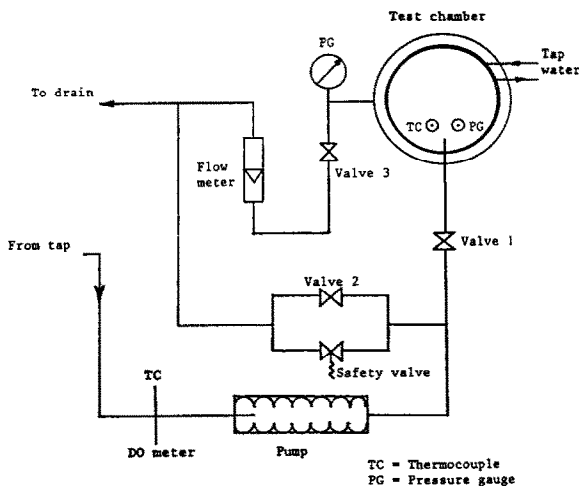

Fig. 2. Schematic of cavitation test rig.

time. The remaining holes were closed with an epoxy resin, whilst dummy stainless steel samples were fitted into the sample slots. The disc was positioned in a cylindrical pressure chamber between two stators which contained radial vanes to prevent excessive water rotation. The positions of the stators were adjustable to allow for the proper disc–stator distance to be selected. A transparent window was situated in the lid of the pressure chamber, in such a position that the cavitating regions on the disc could be viewed with the aid of a stroboscope. A 30 kW two-pole electric motor (natural frequency, 2910 rev min^{-1}) rotated the disc via a belt and pulley system. The disc speed was varied by using different pulley size ratios. Water was pumped through the test chamber by means of a 2 MPa, 30 l min^{-1} screw-type pump. Pressure and flow rate were controlled by hand-operated butterfly valves. Water could be recirculated through the test chamber — for this purpose the flow system included a 100 l reservoir — or passed through only once. In order to cater for chemically corrosive waters, the disc, test chamber, stators, drive shaft, valves, reservoir and all connections were made of stainless steel, while pump components were nickel plated. The flow system was completed by reinforced high-pressure rubber hose.

Heating of the water was required to reach the test temperature, which was mostly above ambient; this was facilitated by a 3 kW heating element in the reservoir. To control temperature rises caused by disc operation, cooling was also necessary. This was supplied by two facilities: a stainless steel cooling coil running around the inside perimeter of the test chamber and a shell-and-tube heat exchanger situated in the flow loop.

2.2. Sample preparation

The test samples were made of AA type 1200 aluminium alloy (known as BS 1C in the UK and Al99,0 in Germany) in the A4 annealed condition, of which

TABLE 1. Specified parameter ranges for rotating disc test rig

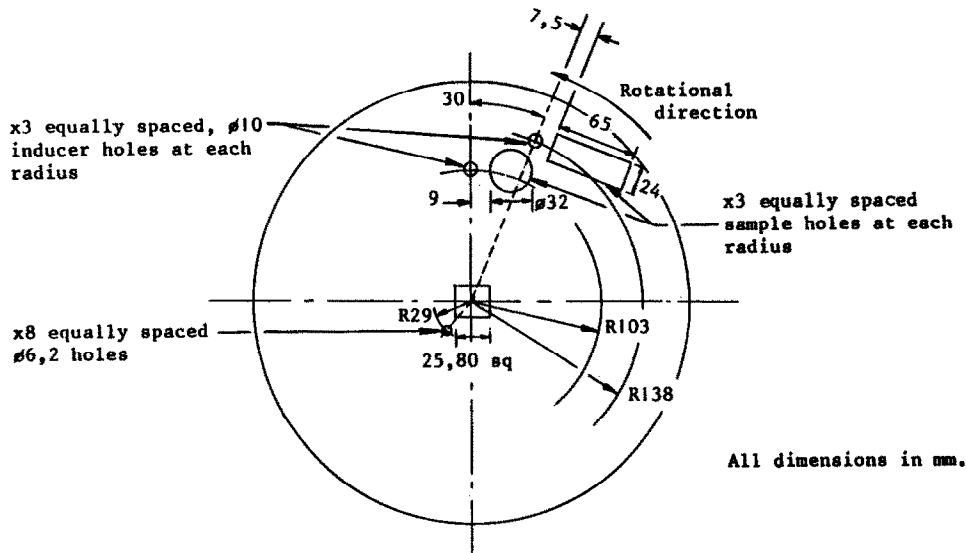| Parameter	Range	Comment
Static water pressure	0.1–2 MPa	
Water temperature	Ambient to 100 °C	
Sample velocity	≈40–60 m s^{-1}	Based on disc velocity, i.e. assuming test fluid to be stationary
Air content of water	Deaerated to supersaturated	Measured as dissolved oxygen content
Water flow rate	0–30 l min^{-1}	
Water quality	neutral to corrosive and containing abrasive solids	To simulate typical mine waters

Fig. 3. Disc design for three rectangular and three roundsamples.

TABLE 2. Composition and typical mechanical properties of AA 1200 Al alloy, H4' annealed condition[a]

Chemical composition									Mechanical properties		
Al	Cu	Mg	Si	Fe	Mn	Zn	Ti	Cr	0.2% Proof stress (MPa)	Tensile strength (MPa)	Elongation in 50 mm (%)
<99.0	0.05	–	Fe + Si 1.0		0.05	0.1	0.05	–	105	125	8

[a]Strain hardened. Material subjected to the application of cold work after annealing (or hot forming), or to a combination of cold work and partial annealing/stabilising in order to secure the specified mechanical properties. H2, H4, H6 etc. indicates ascending order of tensile strength.

the composition and mechanical properties are listed in Table 2.

Rectangular samples, 65 mm × 24 mm and 4 mm thick, were machined to fit tightly into the disc. The surfaces exposed to cavitation were ground and polished to $R_a \sim 0.1 \ \mu$m. The samples were stored in a dry desiccator when not being tested.

2.3. Procedure for erosion testing

The three rectangular sample positions on the front (window) side of the disc were used. The samples were eroded for 1 h in tap water at sample velocities of 48 and 51 m s^{-1} and static water pressures of 0.10, 0.12, 0.135, 0.15 and 0.25 MPa. (Not all combinations of velocity and pressure were tested.) The other test parameters were kept constant at the following values: water temperature, 53 °C; dissolved oxygen content of the water (used as an indication of the air content behaviour), 6.7 mg l^{-1}; water flow rate, 30 l min^{-1}.

Before and after each test the samples were cleaned in ethanol, dried and weighed to the nearest 0.1 mg.

The mass loss from each sample was converted to volume loss. Wear rates were calculated from the average volume loss for the three samples.

3. Results and discussion

3.1. Erosion results

The volume loss data as a function of pressure and velocity are detailed in Table 3. The volume losses are plotted in Fig. 4, showing that the volume loss was larger at the higher sample velocity of 51 m s^{-1} compared to a velocity of 48 m s^{-1}. A peak volume loss occurred at approximately 0.12 MPa for both velocities. Thus the general trends reported in the literature were confirmed.

3.2. Cavitation dynamics

The cavitation cloud was studied *in situ* with the aid of a stroboscope (Fig. 5(a)) for various velocity and pressure conditions, and compared with the erosion zone formed on the type 1200 Al alloy samples (Fig.

TABLE 3. Volume loss as a function of pressure and velocity

Test Code	Velocity (m s^{-1})		Static pressure (MPa)		Average 1 h cumulative volume loss (mm^3)
	Mean value	SD[a]	Mean value	SD	
SP6	48.5	0.08	0.10	0	47.3
SP7	48.5	0.10	0.12	0	60.3
SP8	48.6	0.08	0.20	0.007	30.8
SP5	50.9	0.07	0.10	0	76.5
SP1	50.8	0.05	0.12	0.001	99.3
SP4	50.8	0.04	0.137	0.001	91.5
SP2	50.8	0.05	0.15	0.001	86.3
SP3	50.9	0.06	0.25	0.009	30.0

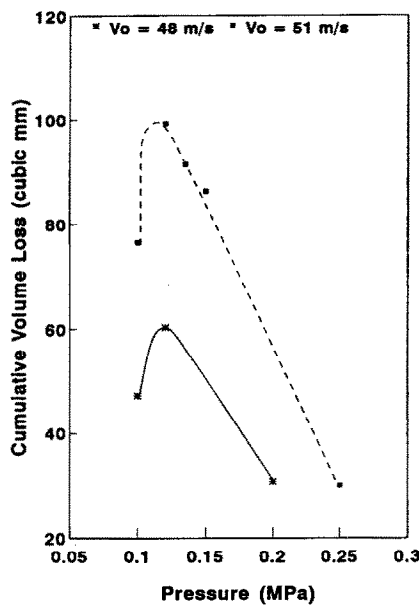[a]SD = standard deviation.

Fig. 4. Curves for volume loss as a function of pressure at 48 and 51 m s^{-1} sample velocity.

Fig. 5. (a) *In situ* observation of the cavitation cloud and (b) erosion zone formed on the samples (A1 to A3). Velocity is 51 m s^{-1} and pressure 0.15 MPa.

5(b)). It was found that each cloud consisted of a "fixed" cavity and "travelling" cavities [12]. A primary erosion pit developed at the downstream end of the fixed cavity. This primary damage zone induced secondary cavitation and damage, the latter forming a "tail" at the downstream side of the primary damage zone.

The cavitation clouds and associated erosion zones are sketched in Fig. 6. Analysis of the figure shows that the cavitation clouds extended farther from the inducer holes with decreasing pressure and increasing velocity, and that the erosion zones moved farther downstream as a result, and vice versa. This is illustrated in Fig. 7, where the position of the erosion zone with respect to the inducer hole is plotted as a function of velocity and pressure. The position of the erosion zone compared to the cavitation cloud was also velocity and pressure dependent, but to a smaller degree (Fig. 8).

The relation between pressure and velocity, cavitation erosion rate and the position of the cavitation damage can be graphically demonstrated in terms of the dynamically created pressure differential. Consider firstly the hypothetical pressure profiles for two different static pressures in Fig. 9(a). Since P_{02} is smaller than P_{01} but constant velocity is assumed, the pressure profile for
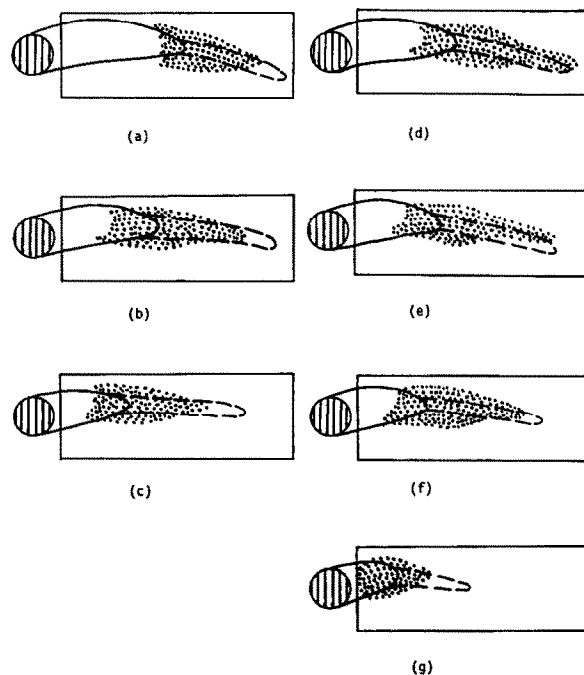

Fig. 6. Cavitation cloud and associated erosion zone for the following sample velocities and static pressures, respectively: (a) 48 m s^{-1} and 0.10 MPa; (b) 48 m s^{-1} and 0.12 MPa; (c) 48 m s^{-1} and 0.135 MPa; (d) 51 m s^{-1} and 0.12 MPa; (e) 51 m s^{-1} and 0.135 MPa; (f) 51 m s^{-1} and 0.15 MPa; (g) 51 m s^{-1} and 0.25 MPa. Fixed and travelling cavities are respectively indicated by solid and dashed lines. The erosion zones are indicated by the dotted areas.
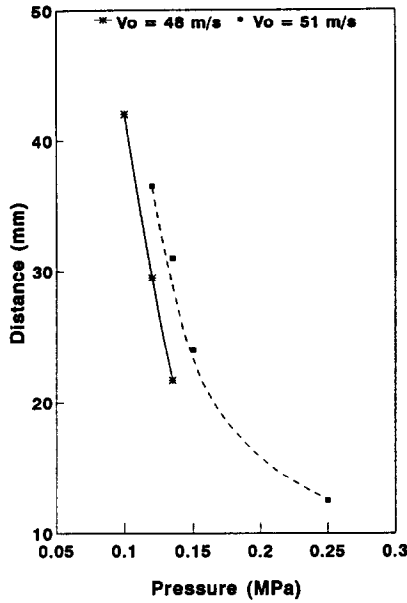
Fig. 7. The distance between the downstream edge of the inducer hole and the centre of the primary erosion zone, plotted as a function of velocity and pressure.
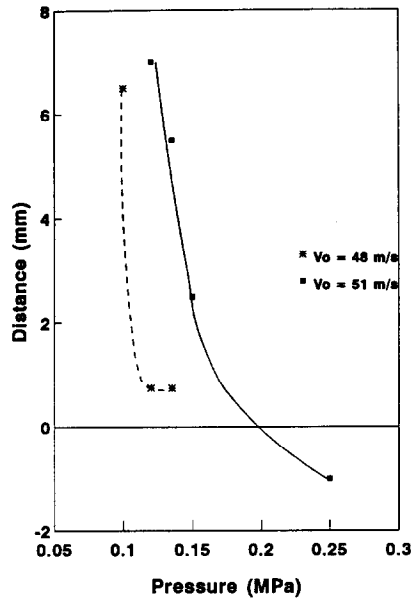

Fig. 8. The distance between the downstream end of the fixed part of the cavitation cloud and the centre of the primary erosion zone, plotted as a function of velocity and pressure.
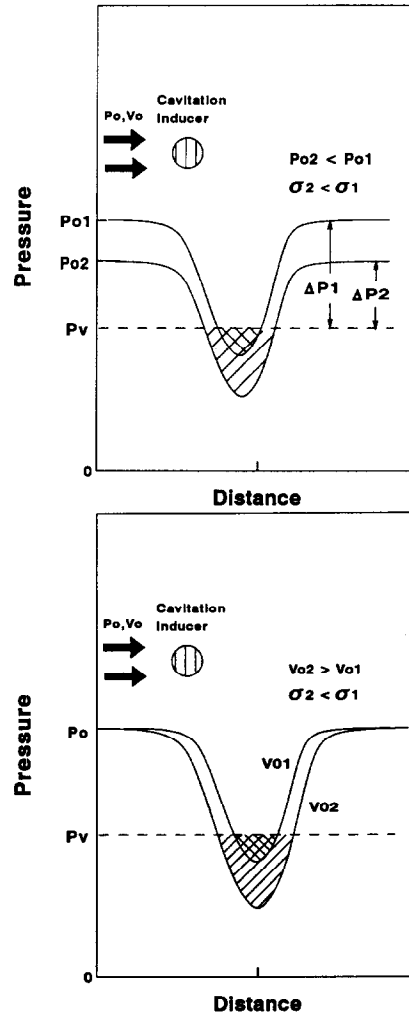

Fig. 9. Hypothetical curves of influence of (a) pressure and (b) velocity on cavitation pressure differential. The cavitation parameter $\sigma = (P_0 - P_v)/(\rho v_0^2/2)$, where ρ is the liquid density, P_0 the undisturbed liquid pressure, P_v the liquid vapour pressure and v_0 the relative velocity of the undisturbed liquid [12].

P_{02} is displaced to lower pressures. As a result, the region of underpressure (hatched area) increases. Thus the cavitation cloud expands in the downstream direction and the erosion zone moves farther downstream.

The number of cavitating bubbles increases at the same time as a result of the larger underpressure region, while the pressure gradient for collapse, i.e. ΔP_2, will decrease. These two opposing factors lead to the existence of a peak damage rate as reported in the literature [1–11].

In the case of two different velocities (Fig. 9(b)), the region of underpressure expands for the higher velocity v_{02}. Thus cavitation bubbles leave this region farther downstream and the erosion zone shifts downstream. At the same time, cavitation damage will increase because of the larger number of cavitating bubbles, as found in previous studies [12–17].

4. Conclusions

The existence of a peak erosion rate as a function of pressure was confirmed by the present results. The erosion rate increased with increasing velocity over the range tested (48 to 51 m s^{-1}).

The pressure and velocity dependence of the erosion rate, and of the geometry of the cavitation cloud and erosion zone, can be explained in terms of the cavitation-inducing, dynamically-created, pressure differential. This relation can be used, for example, to decrease cavitation damage in hydraulic machinery by relocating the erosion zone.

References

1 M.J. Robinson, On the detailed flow structure and the corresponding damage to test specimens in a cavitating Venturi, Ph.D. Thesis, Nuclear Engineering Dept., University of Michigan, 1965.

2 B.C.S. Rao and D.V. Chandrasekhara, Size and Velocity Scale Effects on Damage in a Venturi, Internal Report, Civil Engineering Dept., Bangalore Institute of Technology, 1973.

3 F.G. Hammitt, Observations on cavitation damage in a flowing system, Trans. ASME, J. Basic Eng., 85(D) (1963) 347–359.

4 F.G. Hammitt, L.L. Barinka, M.J. Robinson, R.D. Pehlke and C.A. Siebert, Initial phases of damage to test specimens in a cavitating Venturi, Trans. ASME, J. Basic Eng., 87(D) (1965) 453–464.

5 P. Tullis and R. Govindarajan, Cavitation and size scale effects for orifices, Proc. Paper 9605, J. Hydr. Div., ASCE, 99 (HY3) (1973) 417–430.

6 J.M. Mousson, Pitting resistance of metals under cavitating conditions, Trans. ASME, 59 (1937) 399–408.

7 J.M. Hobbs and A. Laird, Pressure, Temperature and Gas Content Effects in the Vibratory Test, National Engineering Laboratory Report 438, Oct. 1969.

8 S.G. Young and J.R. Johnston, Effect of Cover Gas Pressures on Accelerated Damage in Sodium, NASA TN D-4235, Lewis Research Center, Cleveland, OH, November, 1967.

9 S.G. Young and J.R. Johnston, Accelerated Cavitation Damage of Steels and Superalloys in Liquid Metals, NASA TN D-3226, Lewis Research Center, Cleveland, OH, May, 1966.

10 F.G. Hammitt and D.O. Rogers, Effect of pressure and temperature variation in vibratory cavitation damage test, J. Mech. Eng. Sci., 12(6) (1970) 432–439.

11 F.G. Hammitt and N.R. Bhatt, Cavitation Damage at Elevated Temperature and Pressure, ASME Cavitation and Polyphase Flow Forum, ASME, New York, 1972, pp. 11–13.

12 R.T. Knapp, J.W. Daily and F.G. Hammitt, Cavitation, McGraw-Hill, New York, 1970.

13 R.T. Knapp, Recent investigations of cavitation and cavitation damage, Trans. ASME, 77 (1955) 1045–1054.

14 M.J. Robinson and F.G. Hammitt, Detailed damage characteristics in a cavitating venturi, Trans. ASME, J. Basic Eng., 89(D) (1967) 161–173.

15 R.E.H. Rasmussen, Some experiments on cavitation erosion in water mixed with air, in Cavitation in Hydrodynamics, 20, Proc. NPL Symp. Cavitation in Hydrodynamics, 1955, HMSO, London, 1956.

16 G.M. Wood, L.K. Knudson and F.G. Hammitt, Cavitation studies with rotating disc, Trans. ASME, J. Basic Eng., 89(D) (1967) 98–110.

17 J.Z. Lichtman and E.R. Weingram, The use of a rotating disc apparatus in determining cavitation erosion resistance in materials, ASME Symp. on Cavitation Research Facilities and Techniques, ASME, New York, 1964, pp. 185–196.

18 R.T. Knapp, Recent investigations of cavitation and cavitation damage, Trans. ASME, 77 (1955) 1045–1054.

19 J.Z. Lichtman, D.H. Callas, C.K. Chatten and E.P. Cochran, Cavitation Erosion of Structural Materials and Coatings, 17th Annual Conference, NACE, Buffalo, New York, 1961, pp. 119–127.

20 C.M. Preece, Cavitation erosion, Treatise on Mater. Sci. Tech., Erosion, 16 (1979) 249–308.

21 A. Karimi and J.L. Martin, Cavitation erosion of materials, Int. Met. Rev., 31(1) (1986) 1–26.

22 F.G. Hammitt, Cavitation and Multiphase Flow Phenomena, McGraw-Hill, New York, 1980.

23 R. Canavelis, Contribution a l'Etude de l'Erosion de Cavitation dans les Turbomachines Hydrauliques, Ph.D. Thesis, Faculty of Science, University of Paris, 1966.

24 J.Z. Lichtman, D.H. Kallas, C.K. Chatten and E.P. Cochran Jr., Cavitation erosion of structural materials and coatings, Corrosion, 17 (10) (1961) 119–127.

25 K. Steller, Personal communications with F.G. Hammitt, Institute of Fluid Flow Machines, Polish Academy of Sciences, Gdansk, Poland, 1976.